metals

MDPI

Article

Effect of Superhydrophobic Surface on Corrosion Resistance of Magnesium-Neodymium Alloy in Artificial Hand Sweat

Changyang Liu, Jiapeng Sun and Guosong Wu *

College of Mechanics and Materials, Hohai University, Nanjing 211100, China
* Correspondence: wuguosong@hhu.edu.cn

Abstract: A superhydrophobic surface can endow metals with some intriguing characteristics such as self-cleaning behavior. In this study, a simple solution-immersion method based on the concept of predesigned corrosion is developed to enhance the corrosion resistance of a magnesium-neodymium alloy. The Mg alloy is directly soaked in potassium dihydrogen phosphate solution with the addition of ultrasound, and a layer of rough but dense coating is uniformly formed on the Mg-Nd alloy after the immersion process, which is mainly composed of $MgHPO_4 \cdot 3H_2O$. A superhydrophobic surface with an average wetting angle of 150.5° and a sliding angle of about 4.5° can be obtained on the Mg alloy by further chemical surface modification with perfluorodecyltriethoxysilane. This superhydrophobic surface has an interesting self-cleaning effect as well as good corrosion resistance in artificial hand sweat. In brief, this study provides a feasible way to prepare a superhydrophobic surface on the Mg-Nd alloy and reveals the effect of a superhydrophobic surface on the corrosion behavior of the Mg-Nd alloy, offering new technical insights into the corrosion protection of magnesium alloys.

Keywords: magnesium alloy; surface; coating; self-cleaning; corrosion

check for updates

Citation: Liu, C.; Sun, J.; Wu, G. Effect of Superhydrophobic Surface on Corrosion Resistance of Magnesium-Neodymium Alloy in Artificial Hand Sweat. *Metals* **2023**, *13*, 219. https://doi.org/10.3390/met13020219

Academic Editor: Sebastian Feliú, Jr.

Received: 14 December 2022
Revised: 18 January 2023
Accepted: 20 January 2023
Published: 24 January 2023

1. Introduction

Benefiting from the characteristics of low density, high specific strength and natural biodegradation, magnesium alloys have attracted much attention in the aerospace, transportation, building and biomedical fields [1–6]. However, their poor corrosion resistance in aqueous solutions always hampers their wider applications, which is mainly due to the high chemical activity of magnesium and the loose natural surface film on most magnesium alloys [7–9]. Therefore, it is very crucial to control the corrosion rate of magnesium alloys in engineering applications, and in the past years, surface treatments including electroplating, electroless plating, chemical conversion, thermal spraying, polymer coating, and vapor deposition have been considered among the most effective strategies to enhance their corrosion resistance [10–16].

Zhang et al. proposed a concept for corrosion mitigation of magnesium alloys in which predesigned surface corrosion is conducted before their service. In their study, an effective method was developed using a uniform self-layered coating composed of an inner compact layer and top Mg-Al layered double hydroxide (LDH) micro sheets, prepared on AZ80 Mg alloys in a hydrothermal environment for corrosion protection [17]. Yao et al. immersed a magnesium-neodymium alloy in potassium dihydrogen phosphate solution at 50 °C for 4 h and obtained a layer of uniform $MgHPO_4 \cdot 3H_2O$ coating on the Mg alloy, significantly improving the corrosion resistance of the Mg-Nd alloy in Cl^--containing simulated concrete pore solution [18]. Gradually, it is becoming an acceptable strategy of retarding corrosion that corrosion products may be designed in advance to form a protective surface coating on magnesium alloys. Nonetheless, there have been few studies on the development of this strategy.

Superhydrophobic surfaces are often believed to provide metals with high corrosion resistance because of their ability to repel water [19]. For example, Lin et al. prepared a superhydrophobic Ni-Co/Cu composite coating on carbon steel and successfully improved the corrosion resistance in seawater [20]. In this study, we first immersed an Mg-Nd alloy in KH_2PO_4 solution with the addition of ultrasound to spontaneously form a layer of protective coating based on the aforementioned idea of predesigned corrosion. Then, the surface chemical modification was applied to fabricate a super-hydrophobic surface after the immersion process. Finally, the effect of superhydrophobic surface on the corrosion resistance of Mg-Nd alloy was investigated in artificial hand sweat and the associated corrosion mechanism was also discussed.

2. Materials and Methods

As-cast Mg-3.3 wt. % Nd alloys with dimensions of 10 mm × 10 mm × 5 mm were used as the substrates. The fabrication process of a superhydrophobic surface on the Mg-Nd alloy is shown in Figure 1a. Firstly, Mg-Nd alloys were mechanically ground with silicon carbide abrasive paper up to # 2000, ultrasonically cleaned in ethanol for 3 min, and rapidly dried with air. The samples are denoted as MA. Secondly, three samples were immersed into 120 mL of 0.1 mol·L^{-1} potassium dihydrogen phosphate (KH_2PO_4) solution, whose pH value was equal to 4.6. The solution was heated to 30 °C before the immersion process and the beaker containing this solution was placed in an ultrasonic cleaner during the immersion process. In this process, the samples were treated at a frequency of 100 kHz for 60 min to achieve uniform corrosion. The evolution of temperature and pH value during the treatment are shown in Figure 1b. The samples were taken and washed with deionized water and ethanol in turns, followed by rapid drying. The corresponding samples are denoted as MA/UC. Finally, 2 wt. % perfluorodecyltriethoxysilane ($C_{16}F_{17}H_{19}O_3Si$, PFDS) ethanol solution was prepared with analytical grade reagent PFDS and alcohol. Then, MA/UC samples were soaked in the solution for 2 h. After soaking, the samples were taken out and heated at 140 °C for 1 h in an oven. After drying, the samples were taken out and cooled in the air. Here, the processed samples are named as MA/UC/CM and the MA samples directly modified by 2 wt. % $C_{16}F_{17}H_{19}O_3Si$ ethanol solution are denoted as MA/CM. Figure 1c gives the appearance of all samples, showing that the color of the surface of Mg-Nd alloy changes from bright white to gray-white after the ultrasound-assisted corrosion process.

The surface and cross-section morphologies of the coated samples were observed by scanning electron microscopy (SEM) equipped (Zeiss, Oberkochen, Germany) with energy-dispersive X-ray spectroscopy (EDS) (OXFORD Xplore, Oxford, UK). The phase compositions of the coated and uncoated samples were analyzed by X-ray diffraction (XRD) with Cu Kα radiation. X-ray photoelectron spectroscopy (XPS) with an Al Kα irradiation was conducted to reveal the elemental composition and chemical state of the PFDS-modified surface. The binding energies were referenced to the C 1s peak (284.8 eV).

The static water contact angle and sliding angle of the samples were measured with 4 μL of the ultrapure water droplet on a JC2000D1 instrument (POWEREACH, Shanghai, China). Each static water contact angle was tested at least three different times to calculate the average values. In order to evaluate the self-cleaning ability of the samples, they were placed on a platform with an inclination angle of about 8° and a small amount of grit was uniformly dispersed on their respective surfaces. In the test, blue ink droplets dropped from a height of about 0.01 m above the samples and the state of the grit on the surfaces of different samples was accordingly recorded by a digital camera.

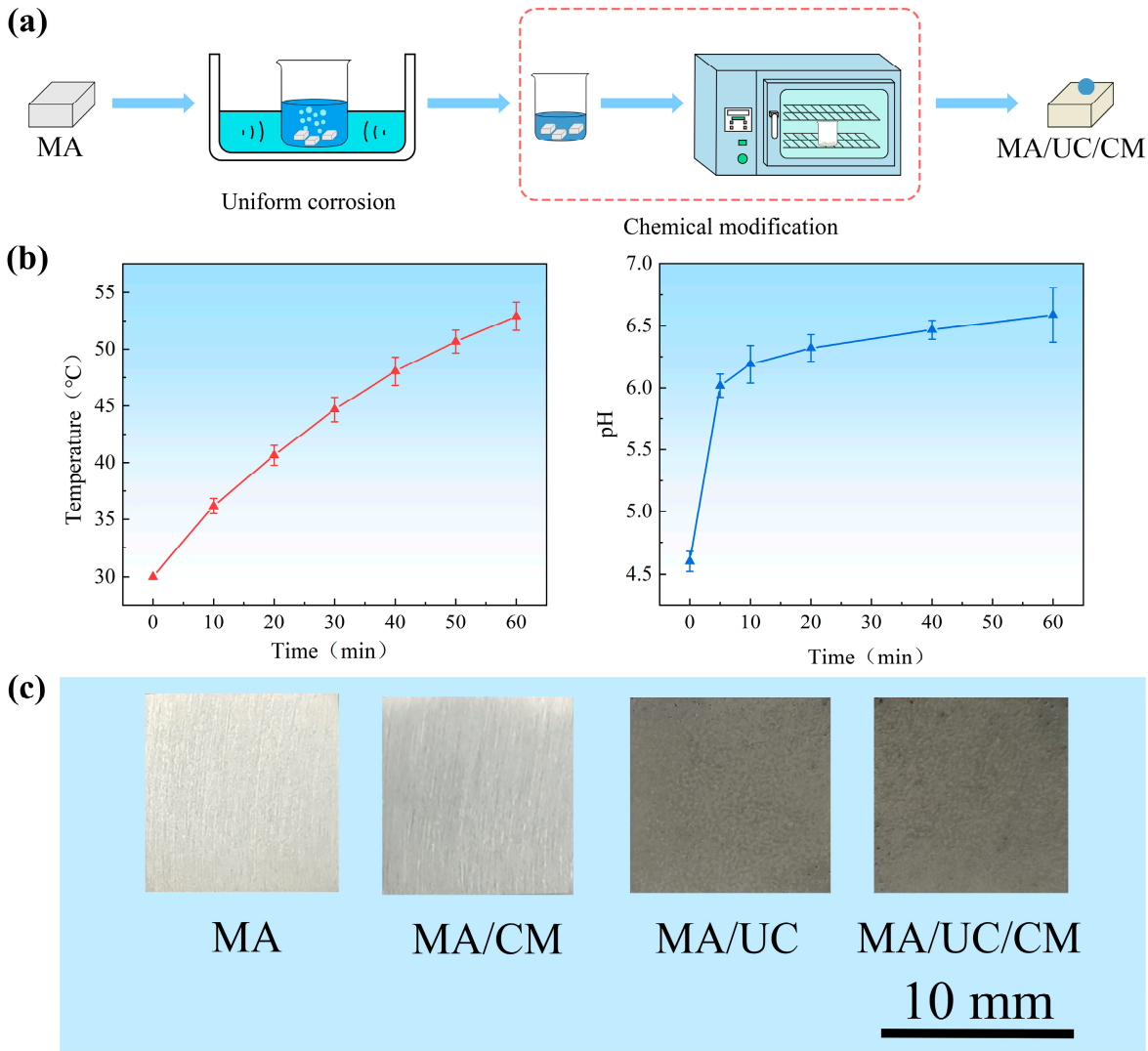

Figure 1. (**a**) Schematic diagram of the fabrication process; (**b**) temperature and pH value evolution during the process; (**c**) surface appearance of the treated and untreated samples.

Corrosion behavior was evaluated by electrochemical measurement and an immersion test in simulated hand sweat. Here, the simulated hand sweat was prepared with a ratio of 0.5 wt.% NaCl, 0.5 wt.% lactic acid and 0.1 wt.% urea. Its pH value was adjusted to 5.5 with 1 mol/L NaOH (pH = 13.01) solution [21–23]. All the electrochemical measurements were carried out on an electrochemical workstation (Reference 600+, Gamry, Warminster, PA, USA) using a conventional three-electrode electrochemical cell. The cell was composed of a sample as the working electrode, a platinum sheet as the counter electrode, and a saturated calomel electrode as the reference electrode. In the test, each sample with an exposed surface area of 1 × 1 cm^2 was immersed in 100 mL of simulated hand sweat for 1 h, and then the electrochemical impedance spectrum (EIS) was collected from 100 kHz to 100 MHz. Similarly, the polarization test was performed at a scanning rate of 1 $mV \cdot s^{-1}$. The corrosion potential (E_{corr}) and corrosion current density (I_{corr}) were derived from the polarization curve, and the impedance data were also fitted using the respective electrical circuits. Furthermore, the immersion test in simulated hand sweat was conducted for evaluating the corrosion resistance of samples. Each investigated sample was immersed in 100 mL of simulated hand sweat and taken out for cleaning and drying after immersion for 24 h. Subsequently, the surface morphology of the corroded samples was captured by scanning electron microscope.

3. Results

Uniform corrosion is one of the key steps to fabricating the superhydrophobic surface on the Mg-Nd alloy in this study. Figure 2 shows the XRD patterns of the pristine sample and the sample treated by uniform corrosion in potassium dihydrogen phosphate solution. It is identified by comparison that the substrate is composed of α phase (Mg) and β phase ($Mg_{12}Nd$) and the newly-formed coating material is $MgHPO_4 \cdot 3H_2O$. Figure 3 exhibits the surface and cross-section morphologies of the coated sample after PFDS modification. It is revealed in Figure 3a,b that the surface consisting of hierarchical regular polygons crystals becomes block-like. The cross-section shown in Figure 3c,d proves that a rough but dense coating is uniformly formed on the surface with an estimated thickness of 27.11 ± 4.44 μm. Figure 4 further shows the EDS elemental mappings of the cross-section, which indicates that the coating mainly contains magnesium, phosphorus, and oxygen. On the one hand, it proves that this composition is in accordance with the result of XRD tests. On the other hand, the distribution of neodymium exhibits the position of β phase ($Mg_{12}Nd$). Generally, most common phosphate conversion coatings have massive cracks due to the dehydration process or the entrapped hydrogen [24,25]. Relatively speaking, the number of cracks in our prepared coating is very small. Furthermore, the crack shown in Figure 4 possibly stems from the process of mechanical polishing for the preparation of SEM samples. Figure 5a shows the XPS survey spectrum of the coated sample after PDFS-modification, which discloses the presence of elements C, F, and Si. Figure 5b–d shows the high-resolution XPS spectra of C 1s, F 1s, and Si 2p, respectively. The F 1s spectrum shows one peak at 688.8 eV, the Si 2p spectrum shows one peak at 102.2 eV, and the C 1s spectrum can be deconvoluted into 4 peaks, namely $-CF_3$ at 293.6 eV, $-CF_2$ at 291.3 eV, -C-O at 286 eV, -C-C at 284.8 eV, suggesting that the surface has been successfully modified by PFDS.

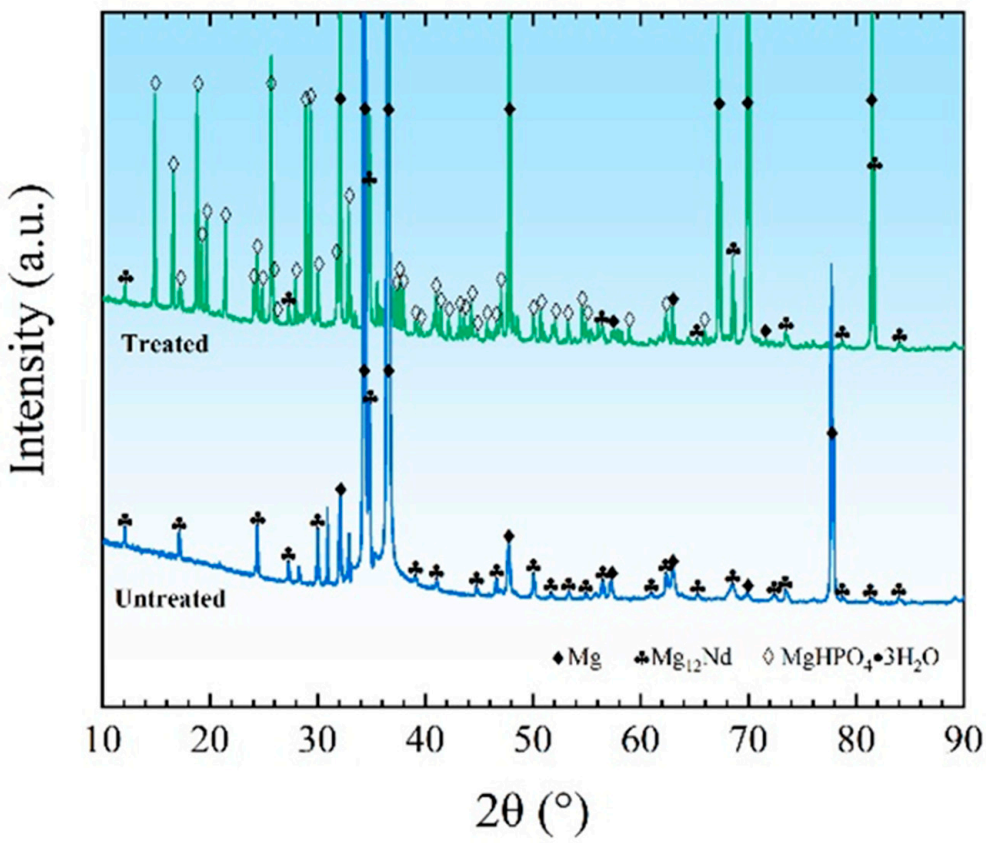

Figure 2. XRD patterns of the untreated sample and the sample treated by uniform corrosion.

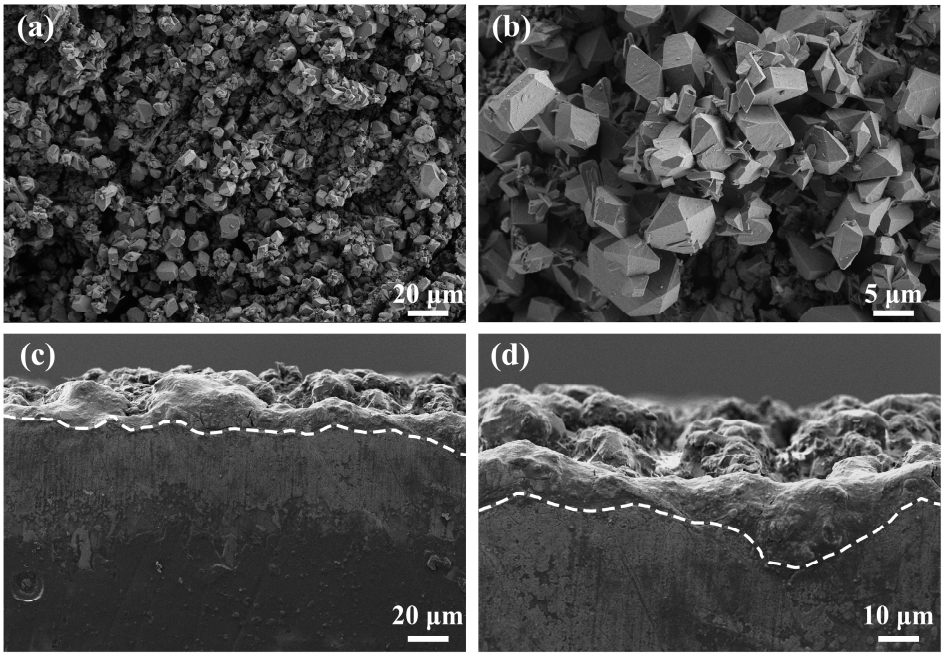

Figure 3. (**a**,**b**) SEM images of surface morphology of the coated sample after PFDS-modification; (**c**,**d**) SEM images of cross-section morphology of the coated sample after PFDS-modification.

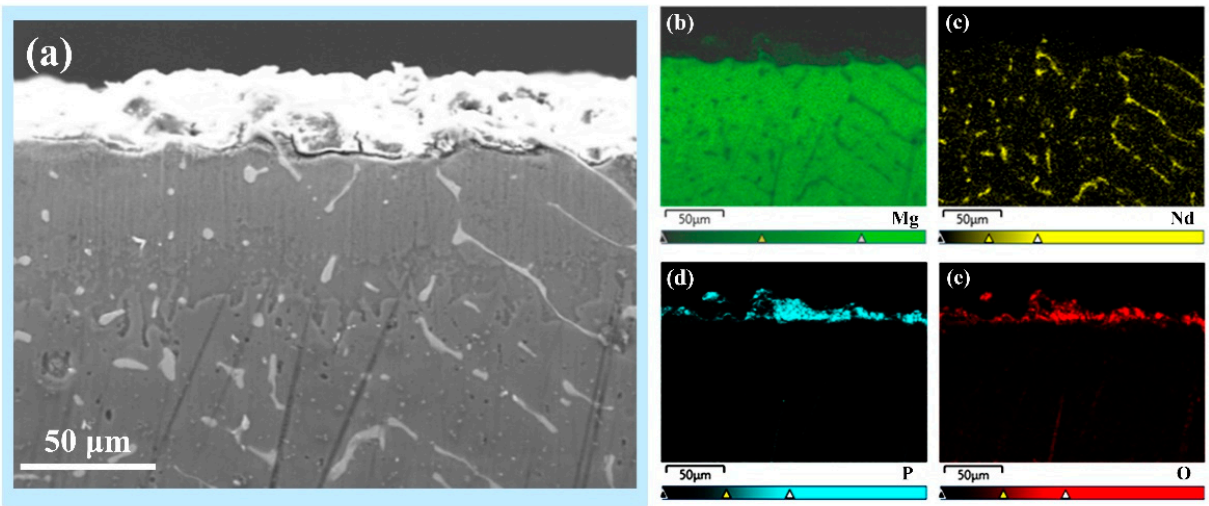

Figure 4. EDS mapping of the cross-section of the coated sample after PFDS-modification: (**a**) SEM image of the selected region, (**b**–**e**) maps showing the distribution of the elements.

Figure 6a shows the macro-wettability of MA, MA/UC, MA/CM, and MA/UC/CM captured by a digital camera. The droplet spreads out on the surface of MA, whereas it is absorbed by the surface of MA/UC. In contrast, the droplet keeps an apparent ball-like shape on MA/CM and MA/UC/CM, respectively. Figure 6b gives the measured contact angles of samples fabricated by different methods. MA, i.e., the Mg-Nd alloy, is hydrophilic with a contact angle of 18.9 ± 2.1° and MA/UC, i.e., the Mg-Nd alloy processed by uniform corrosion, exhibits much stronger hydrophilicity and thus much smaller contact angle, which corresponds to the phenomenon that the blue water droplets are directly absorbed, as shown in Figure 6a. After PFDS-modification, the surfaces of the samples become hydrophobic. The contact angles of MA/CM and MA/UC/CM are 119.5 ± 3.6° and 150.5 ± 0.6°, respectively. In addition, the sliding angles of MA/CM and MA/UC/CM are about 19° and approximately 4.5°, respectively.

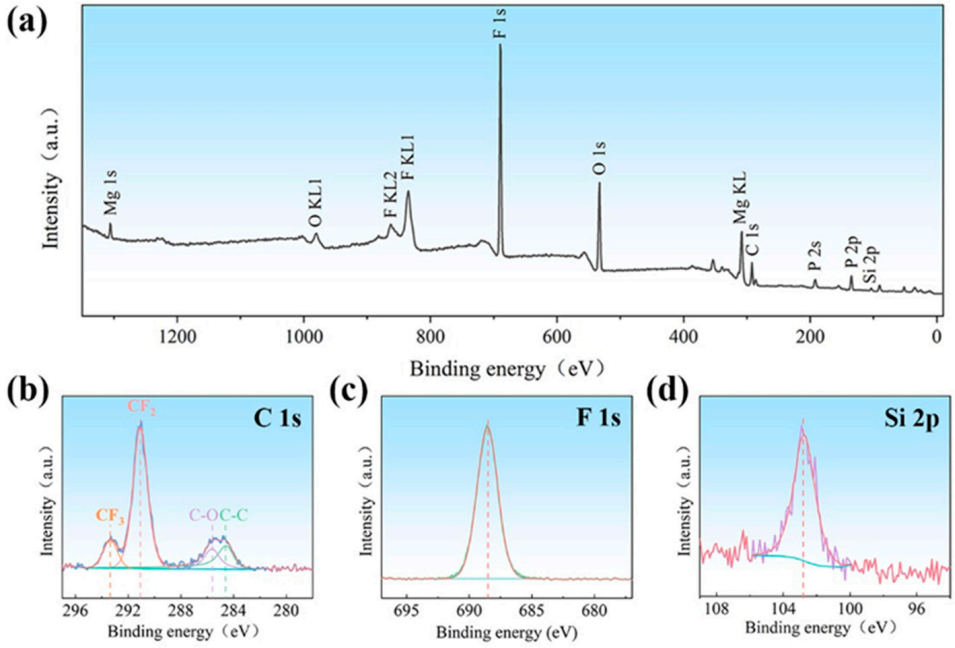

Figure 5. XPS spectra of the PFDS-modified surface: (**a**) survey spectrum and high-resolution spectra of (**b**) C 1s, (**c**) F 1s and (**d**) Si 2p.

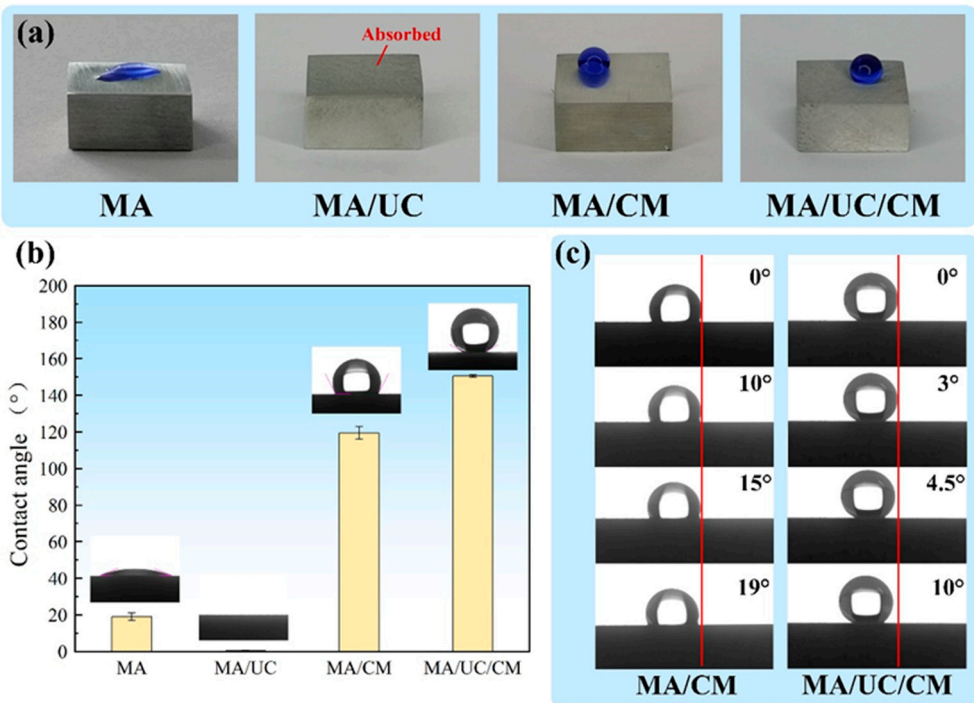

Figure 6. (**a**) Macro-wettability of the investigated samples; (**b**) water contact angle of the investigated samples; (**c**) sliding angle of the hydrophobic samples.

Figure 7a shows the results of the self-cleaning tests that were performed according to the schematic diagram shown in Figure 7b. For MA and MA/UC, the blue water droplet directly infiltrates the grits due to the hydrophilicity of the surfaces. Although the surface of MA/CM is hydrophobic with a contact angle close to 120° and a sliding angle of about 19°, the water droplet cannot roll down from the surface covered with grits because the inclination of the platform is only 8° in this study. In contrast, the water droplet which has fallen on MA/UC/CM can immediately blend with grits and rapidly roll down, taking

away the grits simultaneously. Therefore, it is concluded that the surface of MA/UC/CM has an exclusive self-cleaning effect compared to others.

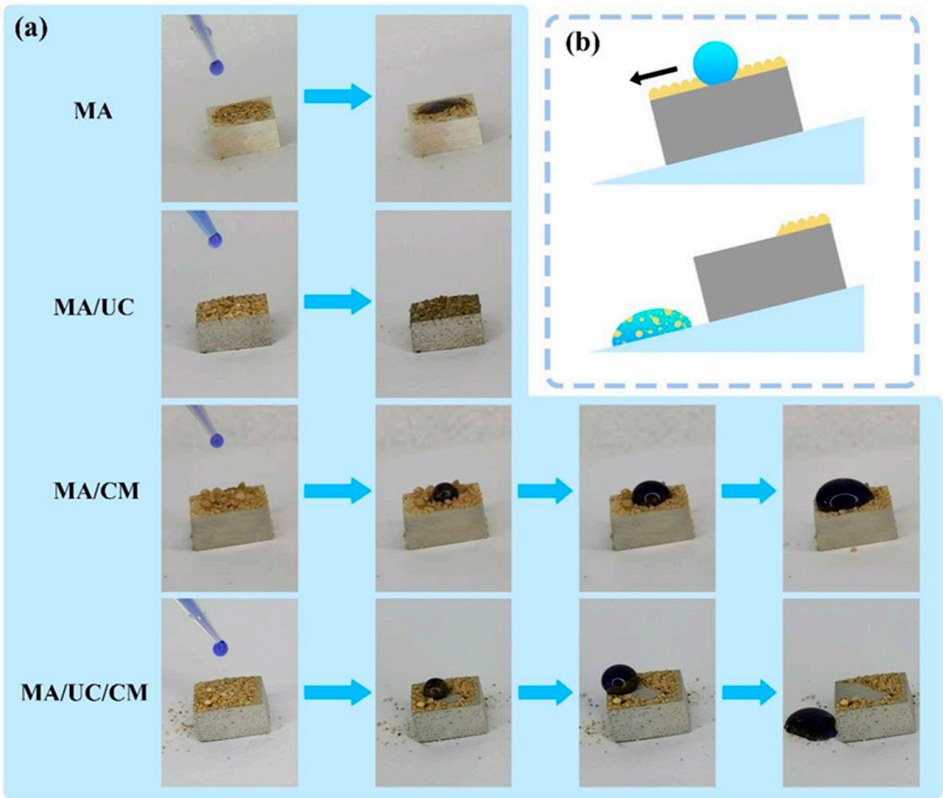

Figure 7. (**a**) Self-cleaning behavior of all the investigated samples; (**b**) schematic diagram of the test.

Figure 8a presents the polarization curves of all the investigated samples after immersion in artificial hand sweat for 1 h. The average corrosion potential (E_{corr}) and corrosion current density (I_{corr}) calculated from polarization curves are summarized in Figure 8b. The corrosion potential of MA is comparable to that of MA/CM, but both are far lower than those of MA/UC and MA/UC/CM, indicating that the $MgHPO_4 \cdot 3H_2O$ coating can significantly improve the corrosion potential of the alloy. In addition, MA/UC/CM exhibits the lowest corrosion current density and the corrosion current density of MA/CM is comparable to that of MA/UC. Since smaller I_{corr} corresponds to better corrosion resistance [26], this indicates that MA/UC/CM has the best corrosion resistance among all the samples.

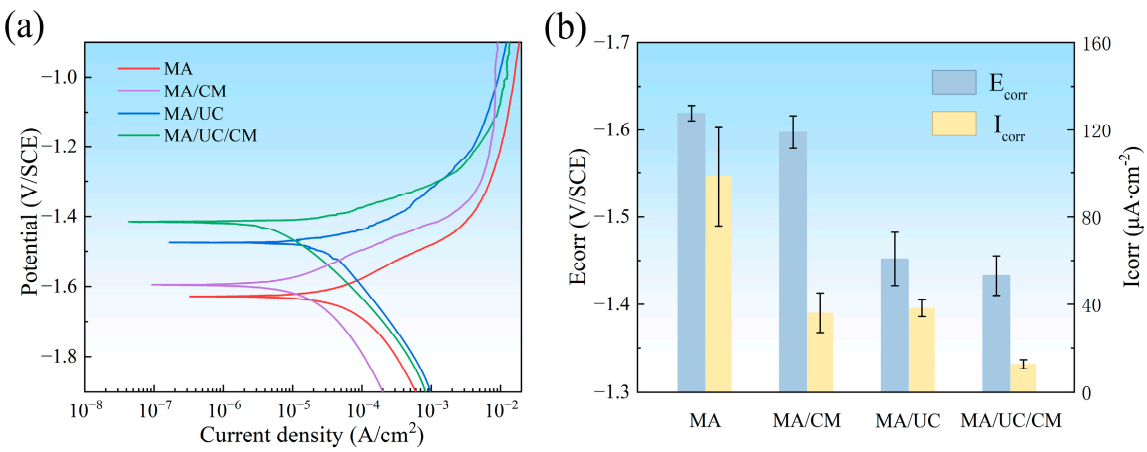

Figure 8. (**a**) Polarization curves of all the investigated samples after immersion for 1 h; (**b**) E_{corr} and I_{corr} calculated from the corresponding polarization curves.

Figure 9 shows the electrochemical impedance spectroscopy of all the samples after immersion in artificial hand sweat for 1 h. Figure 9a,b give the Bode plots and Nyquist plots, respectively. The impedance at the lowest frequency is generally used to estimate corrosion resistance, and a bigger impedance at the lowest frequency means better corrosion resistance [27,28]. As shown in Figure 9a, MA/UC/CM has the highest impedance and MA has the lowest one at the frequency of 100 mHz in the Bode plots. In addition, the impedance of MA/CM at the frequency of 100 mHz is close to that of MA/UC. The results of the Nyquist plots are in accordance with those of the Bode plots. Three equivalent circuits in Figure 9d are proposed for fitting those spectra based on the previous literature [27–29]. $R_s(Q_{dl}\ R_{ct})(Q_{diff}\ R_{diff})$ is used to fit the EIS data of MA and MA/CM, $R_s(Q_f(R_{pore}(Q_{dl}\ R_{ct})(Q_{diff}\ R_{diff})))$ is used in an attempt to fit the EIS data of MA/UC, and $R_s(Q_f(R_{pore}(Q_{dl}\ (R_{ct}(Q_{diff}\ R_{diff})))))$ is applied to fit the one of MA/UC/CM. In the aforementioned circuits, R_s refers to the solution resistance, Q_{dl} and R_{ct} represent the electric double layer capacity and the charge transfer resistance, respectively. Q_{diff} represents the capacitance pertaining to the diffusion and R_{diff} denotes the relevant resistance. Q_f refers to the capacitance of the whole film and R_{pore} represents the total resistance of the pores in the whole film. The fitting data and calculated polarization resistance R_p are listed in Table 1. Generally, the polarization resistance R_p is believed to be used to evaluate the corrosion resistance, i.e., the larger R_p is, the better the corrosion resistance is [26,27,30,31]. Consequently, it is concluded that MA/UC/CM has the best corrosion resistance due to having the highest polarization resistance, which also agrees well with the estimation from the Bode plots.

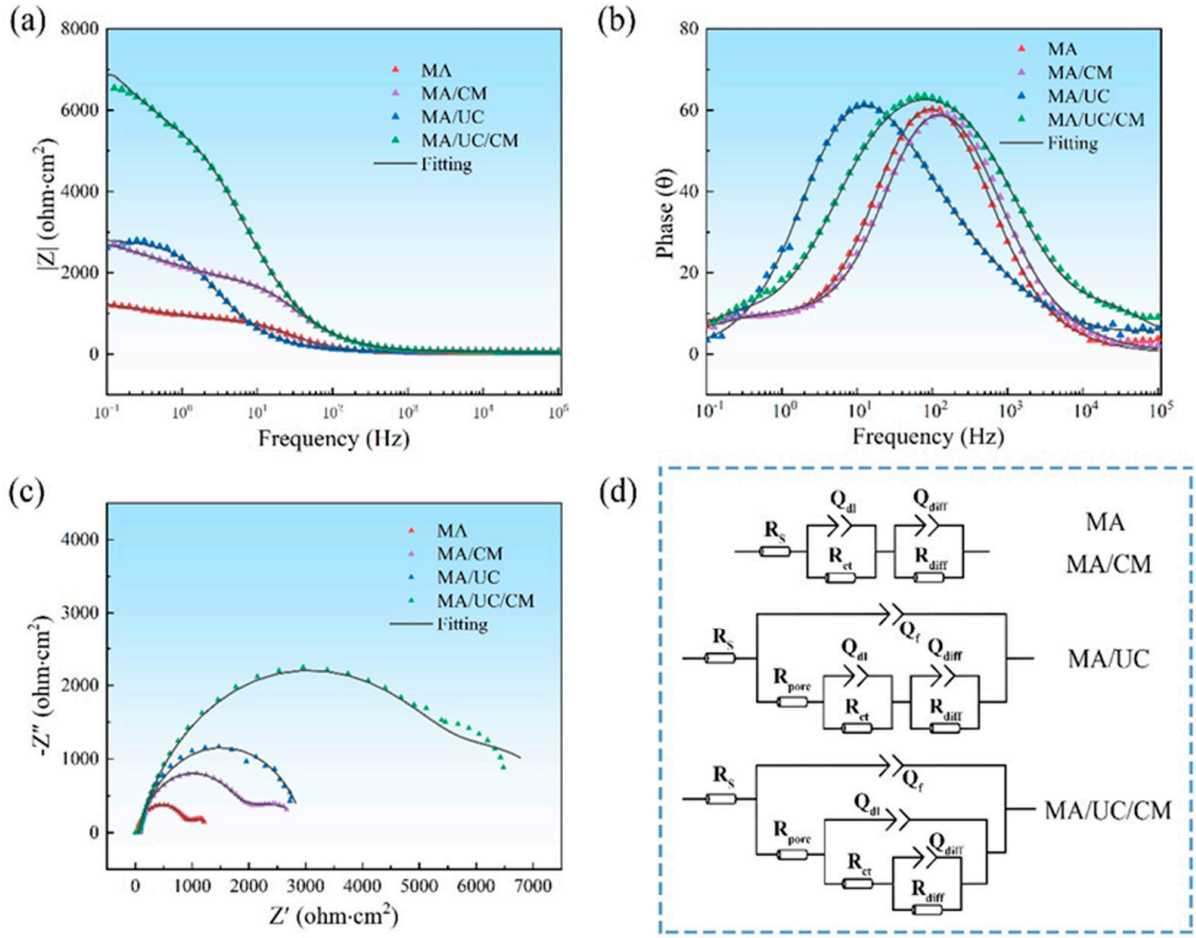

Figure 9. (**a**) Bode plots of the sample after immersion for 1 h: impedance versus frequency; (**b**) Bode plots of the sample after immersion for 1 h: phase angle versus frequency; (**c**) Nyquist plots of the sample after immersion for 1 h; (**d**) equivalent electrical circuits models for the investigated samples.

Table 1. Fitted EIS data based on the equivalent circuits.

Sample		MA	MA/CM	MA/UC	MA/UC/CM
	R_s ($\Omega \cdot cm^2$)	42 ± 6	55 ± 21	37 ± 2	44 ± 1
Q_f	Y_f ($\Omega^{-1} \cdot cm^{-2} \cdot s^n$)	/	/	$(1.42 \pm 0.36) \times 10^{-5}$	$(1.76 \pm 0.01) \times 10^{-6}$
	n_f	/	/	0.60 ± 0.02	0.83 ± 0.02
	R_{pore} ($\Omega \cdot cm^2$)			7 ± 4	31 ± 3
Q_{dl}	Y_d ($\Omega^{-1} \cdot cm^{-2} \cdot s^n$)	$(1.41 \pm 0.10) \times 10^{-3}$	$(5.14 \pm 0.73) \times 10^{-4}$	$(7.72 \pm 2.81) \times 10^{-4}$	$(8.31 \pm 0.09) \times 10^{-6}$
	n_{dl}	0.75 ± 0.18	0.70 ± 0.23	0.45 ± 0.05	0.81 ± 0.01
	R_{ct} ($\Omega \cdot cm^2$)	781 ± 92	1566 ± 125	555 ± 389	5105 ± 753
Q_{diff}	Y_{diff} ($\Omega^{-1} \cdot cm^{-2} \cdot s^n$)	$(1.38 \pm 0.09) \times 10^{-5}$	$(5.31 \pm 0.77) \times 10^{-6}$	$(2.81 \pm 0.18) \times 10^{-5}$	$(2.99 \pm 1.81) \times 10^{-3}$
	n_{diff}	$(1.41 \pm 0.10) \times 10^{-3}$	0.80 ± 0.26	0.98 ± 0.02	0.91 ± 0.01
	R_{diff} ($\Omega \cdot cm^2$)	713 ± 48	1668 ± 216	2204 ± 433	1172 ± 346
	R_p ($\Omega \cdot cm^2$)	1494 ± 45	3234 ± 322	2766 ± 45	7339 ± 1188

Figure 10 shows the surface morphology of all the investigated samples after immersion in simulated hand sweat for 24 h. After immersion for 24 h, MA, MA/CM and MA/UC exhibit severe damage on their respective surfaces, especially big corrosion pits occurring on MA and MA/UC. SEM observation reveals that localized corrosion such as pits dominates the damage mode of MA and MA/UC (Figure 10a,c), whereas MA/CM presents web-like localized corrosion with some tiny cracks (Figure 10b). Fortunately, there is no obvious damage on the surface of MA/UC/CM from the macroscopic observation and even under the observation of SEM, the substrate is still completely covered by the coating though there is slight uniform corrosion of the coating in simulated hand sweat. The result further corroborates that the super-hydrophobic Mg-P coating can significantly enhance the corrosion resistance of the magnesium-neodymium alloy.

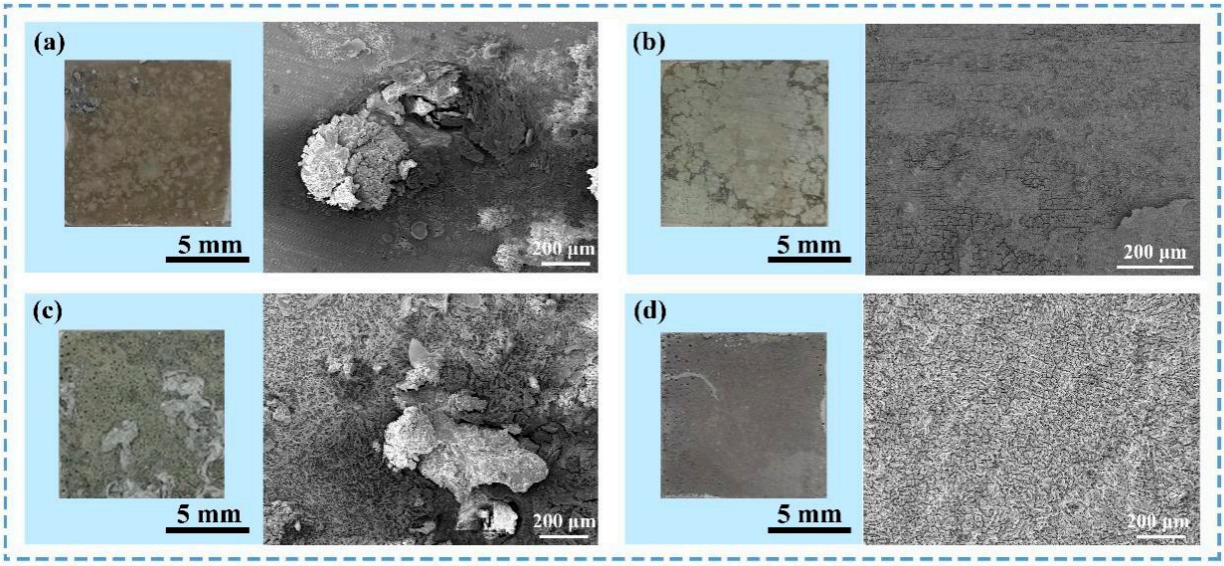

Figure 10. Optical and SEM images of surface morphology of (**a**) MA, (**b**) MA/CM, (**c**) MA/UC and (**d**) MA/UC/CM after immersion for 24 h.

4. Discussion

Yuan et al. introduced Nd, one of the light rare earth elements, into magnesium alloys for improving their mechanical properties by solid solution strengthening and precipitation strengthening and successfully developed a kind of Mg-Nd-Zn-Zr alloy (denoted as JDBM) mainly consisting of α-Mg and $Mg_{12}Nd$ for biomedical applications [32–34]. The corrosion potential of $Mg_{12}Nd$ is slightly more positive than that of α-Mg and the small potential difference between them is believed to slow down galvanic corrosion and thus lead to

highly uniform degradation under physiological conditions [33,35,36]. In our study, the microstructure of the investigated Mg-Nd alloys is extremely similar to that of the JDBM alloy, providing the feasibility of uniform corrosion in potassium dihydrogen phosphate (KH_2PO_4) solution for forming a uniform protective coating.

Figure 11a,b show the schematic diagram of the coating formation. The coating formation mechanism from the perspective of chemical reactions is discussed below: firstly, H^+ and HPO_4^{2-} are ionized from $H_2PO_4^-$ in the solution. Then, the Mg matrix rapidly reacts with H^+ in the solution to generate H_2 due to its high chemical activity, giving rise to the rapid increase of the pH value during the coating process. Subsequently, Mg^{2+}, HPO_4^- and water are combined and deposited on the surface of the substrate. The associated chemical reactions are shown as follows [18,37,38]:

$$H_2PO_4^- \rightarrow H^+ + HPO_4^{2-} \quad (1)$$

$$Mg + 2H^+ \rightarrow Mg^{2+} + H_2 \uparrow \quad (2)$$

$$Mg^{2+} + HPO_4^{2-} + 3H_2O \rightarrow MgHPO_4 \cdot 3H_2O \quad (3)$$

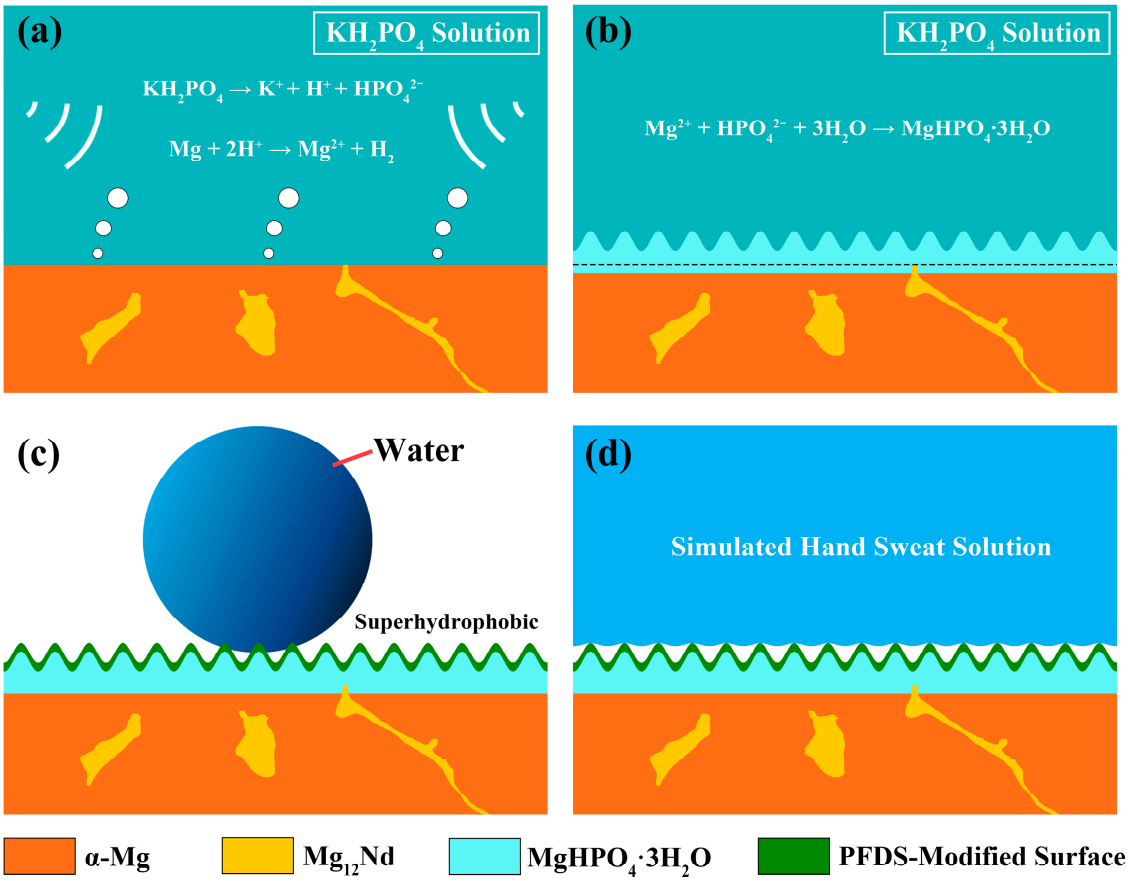

Figure 11. (**a**,**b**) Schematic diagram of the coating formation during ultrasonic-assisted chemical conversion; (**c**) superhydrophobic surface on Mg-Nd alloy; (**d**) anti-corrosion mechanism in artificial hand sweat solution.

During the coating process, the magnesium matrix is corroded and dissolved into KH_2PO_4 solution, and the second phases, $Mg_{12}Nd$, remain undissolved. Here, some second phases may be encapsulated in the corrosion products ($MgHPO_4 \cdot 3H_2O$), which is revealed in the cross-sectional EDS mapping (Figure 3).

Ultrasound is known to play an effective role in coating formation. For example, Lv et al. introduced ultrasonic vibration into the micro-arc oxidation process for fabricating

Zn-modified TiO_2 coating. With the help of ultrasonic vibration, a uniform surface layer was successfully produced to enhance corrosion resistance, increase adhesive strength and improve biological performance [39]. In our study, it is speculated that the generation and bursting of H_2 will lead to the non-synchronous deposition of $MgHPO_4 \cdot 3H_2O$ on the surface. Thus, the coating becomes rough enough to establish a necessary condition for obtaining the superhydrophobic behavior.

Figure 11c shows a schematic diagram explaining the superhydrophobic behavior of the coating. A suitable rough microstructure has been constructed on the surface of the Mg-Nd alloy. Usually, polysiloxane catching oxhydryl on the surface of materials can form an effective bonding and exposed perfluoroalkyl groups can reduce the surface free energy of materials to achieve the hydrophobic effect [40]. After the surface modification with PFDS, one of the low surface energy materials, the surface has acquired sufficient conditions for superhydrophobic behavior. The water static contact angle on MA/UC/CM is greater than 150° and the sliding angle is less than 10°, thus indicating that water droplets can easily roll off the surface once they contact the sample. Moreover, a superhydrophobic surface has a small fraction of the solid/liquid contact area, inducing a lot of air pockets trapped underneath the liquid [17,19,41,42]. Based on the nature of superhydrophobic behavior, the anti-corrosion mechanism of the coating in artificial hand sweat solution can be inferred (Figure 11d). If the surface is immersed in artificial hand sweat, air pockets will be formed among the rough structure to reduce the actual contact between the sample and the external medium. Consequently, the water-repellent behavior integrated with the barrier effect of the coating can prevent the corrosion of the substrate in artificial hand sweat significantly, based on the findings of this study.

In summary, a facile process has been successfully developed to form an anti-corrosion coating on an Mg-Nd alloy based on the concept of predesigned corrosion. This coating with chemical modification can not only improve the corrosion resistance but also exhibit a good self-cleaning effect. Nonetheless, this strategy needs to be refined to produce more effective techniques in the future for actual applications. For instance, the range of substrate materials should be expanded to other commercial alloys and the sustainability of the coating in artificial hand sweat solution should be further improved.

5. Conclusions

In this study, a superhydrophobic coating was successfully fabricated on a magnesium-neodymium alloy by ultrasonic-assisted immersion process and post chemical surface modification. The immersion process can generate a layer of rough but dense $MgHPO_4 \cdot 3H_2O$ coating on the Mg-Nd alloy and post chemical surface modification is responsible for resulting in the super-hydrophobic behavior. The contact angle of the super-hydrophobic coating is $150.5 \pm 0.6°$ and the sliding angle is about 4.5°, which endows the surface of the Mg-Nd alloy with an excellent self-cleaning effect. Both electrochemical measurement and immersion testing show that the Mg-Nd alloy samples with a super-hydrophobic surface have significantly improved corrosion resistance in artificial hand sweat compared to the samples without a super-hydrophobic effect. This study provides an effective strategy for corrosion mitigation of magnesium alloys.

Author Contributions: Conceptualization, G.W.; methodology, C.L. and J.S.; investigation, C.L.; resources, G.W.; data curation, C.L.; writing—original draft preparation, C.L.; writing—review and editing, G.W.; visualization, C.L.; supervision, G.W.; project administration, J.S.; funding acquisition, G.W. All authors have read and agreed to the published version of the manuscript.

Funding: This research was funded by the National Natural Science Foundation of China, grant number 51971088, and the Fundamental Research Funds for the Central Universities of China, grant number 2017B05914.

Data Availability Statement: The data presented in this study are available on request from the corresponding author.

Conflicts of Interest: The authors declare no conflict of interest.

References

1. Xu, W.; Birbilis, N.; Sha, G.; Wang, Y.; Daniels, J.E.; Xiao, Y.; Ferry, M. A high-specific-strength and corrosion-resistant magnesium alloy. *Nat. Mater.* **2015**, *14*, 1229–1235. [CrossRef] [PubMed]
2. Ogawa, Y.; Ando, D.; Sutou, Y.; Koike, J. A lightweight shape-memory magnesium alloy. *Science* **2016**, *353*, 368–370. [CrossRef] [PubMed]
3. Trang, T.; Zhang, J.; Kim, J.; Zargaran, A.; Hwang, J.; Suh, B.; Kim, N. Designing a magnesium alloy with high strength and high formability. *Nat. Commun.* **2018**, *855*, 143901. [CrossRef] [PubMed]
4. Proust, G. Processing magnesium at room temperature. *Science* **2019**, *365*, 30–31. [CrossRef]
5. Feng, H.; Wang, G.; Jin, W.; Zhang, X.; Huang, Y.; Gao, A.; Wu, H.; Wu, G.; Chu, P. Systematic study of inherent anti-bacterial properties of magnesium-based biomaterials. *ACS Appl. Mater. Interfaces* **2016**, *8*, 9662–9673. [CrossRef]
6. Wang, Y.; Wu, G.; Sun, J. Improved corrosion resistance of magnesium alloy in simulated concrete pore solution by hydrothermal treatment. *Scanning* **2020**, *2020*, 4860256. [CrossRef]
7. Cao, F.; Song, G.; Atrens, A. Corrosion and Passivation of Magnesium Alloys. *Corros. Sci.* **2016**, *111*, 835–845. [CrossRef]
8. Li, X.; Liu, X.; Wu, S.; Yeung, K.; Zheng, Y.; Chu, P. Design of magnesium alloys with controllable degradation for biomedical implants: From bulk to surface. *Acta Biomater.* **2016**, *45*, 2–30. [CrossRef]
9. Wu, G.; Ibrahim, J.; Chu, P. Surface design of biodegradable magnesium alloys—A review. *Surf. Coat. Technol.* **2013**, *233*, 2–12. [CrossRef]
10. Zhang, Z.; Yu, G.; Ouyang, Y.; He, X.; Hu, B.; Zhang, J.; Wu, Z. Studies on influence of zinc immersion and fluoride on nickel electroplating on magnesium alloy AZ91D. *Appl. Surf. Sci.* **2009**, *255*, 7773–7779. [CrossRef]
11. Shang, W.; Zhan, X.; Wen, Y.; Li, Y.; Zhang, Z.; Wu, F.; Wang, C. Deposition mechanism of electroless nickel plating of composite coatings on magnesium alloy. *Chem. Eng. Sci.* **2019**, *207*, 1299–1308. [CrossRef]
12. Harada, Y.; Kumai, S. Effect of ceramics coating using sol–gel processing on corrosion resistance and age hardening of AZ80 magnesium alloy substrate. *Surf. Coat. Technol.* **2013**, *228*, 59–67. [CrossRef]
13. Chiu, L.; Chen, C.; Yang, C. Improvement of corrosion properties in an aluminum-sprayed AZ31 magnesium alloy by a post-hot pressing and anodizing treatment. *Surf. Coat. Technol.* **2005**, *191*, 181–187. [CrossRef]
14. Surmeneva, M.; Vladescu, A.; Cotrut, C.; Tyurin, A.; Pirozhkova, T.; Shuvarin, I.; Elkin, B.; Oehr, C.; Surmenev, R. Effect of parylene C coating on the antibiocorrosive and mechanical properties of different magnesium alloys. *Appl. Surf. Sci.* **2018**, *427*, 617–627. [CrossRef]
15. Alphonse, M.; Raja, V.; Gupta, M. Optimization of plasma nitrided, liquid nitrided & PVD TiN coated H13-D2 friction drilling tool on AZ31B magnesium alloy. *Mater. Today Proc.* **2021**, *46*, 9520–9528.
16. Wu, G. Fabrication of Al and Al/Ti coatings on magnesium alloy by sputtering. *Mater. Lett.* **2007**, *61*, 3815–3817. [CrossRef]
17. Zhang, X.; Wu, G.; Peng, X.; Li, L.; Feng, H.; Gao, B.; Huo, K.; Chu, P. Mitigation of corrosion on magnesium alloy by predesigned surface corrosion. *Sci. Rep.* **2015**, *5*, 17399. [CrossRef] [PubMed]
18. Yao, X.; Yang, Y.; Zheng, M.; Wang, J.; Liu, C.; Sun, J.; Wu, G. Enhanced corrosion resistance of magnesium-neodymium alloy in simulated concrete pore solution by predesigned corrosion product. *Mater. Today Commun.* **2022**, *32*, 104027. [CrossRef]
19. Feng, L.; Zhu, Y.; Wang, J.; Shi, X. One-step hydrothermal process to fabricate superhydrophobic surface on magnesium alloy with enhanced corrosion resistance and self-cleaning performance. *Appl. Surf. Sci.* **2017**, *422*, 566–573. [CrossRef]
20. Lin, Z.; Zhang, W.; Zhang, W.; Xu, L.; Xue, Y.; Li, W. Fabrication of Ni–Co/Cu super-hydrophobic coating with improved corrosion resistance. *Mater. Chem. Phys.* **2022**, *277*, 125503. [CrossRef]
21. Hui, J.; O'Dell, Z.J.; Rao, A.; Riley, K.R. In situ quantification of silver nanoparticle dissolution kinetics in simulated sweat using linear sweep stripping voltammetry. *Environ. Sci. Technol.* **2019**, *53*, 13117–13125. [CrossRef] [PubMed]
22. Qian, X.; Gu, Z.; Tang, Q.; Hong, A.; Xu, Z.; Dai, Y.; Bian, X.; Lou, H.; Mortimer, M.; Baalousha, M.; et al. Chemical transformations of nanoscale zinc oxide in simulated sweat and its impact on the antibacterial efficacy. *J. Hazard. Mater.* **2021**, *410*, 124568. [CrossRef] [PubMed]
23. Wang, W.; Zhang, X.; Wu, G.; Wang, C.; Chu, P. Praseodymium-surface-modified magnesium alloy: Retardation of corrosion in artificial hand sweat. *Mater. Lett.* **2016**, *163*, 85–89. [CrossRef]
24. Zhou, W.; Shan, D.; Han, E.; Ke, W. Structure and formation mechanism of phosphate conversion coating on die-cast AZ91D magnesium alloy. *Corros. Sci.* **2008**, *50*, 329–337. [CrossRef]
25. Zhou, P.; Yu, B.; Hou, Y.; Duan, G.; Yang, L.; Zhang, B.; Zhang, T.; Wang, F. Revisiting the cracking of chemical conversion coating on magnesium alloys. *Corros. Sci.* **2021**, *178*, 109069. [CrossRef]
26. Xu, B.; Sun, J.; Han, J.; Yang, Z.; Zhou, H.; Xiao, L.; Xu, S.; Han, Y.; Ma, A.; Wu, G. Effect of hierarchical precipitates on corrosion behavior of fine-grain magnesium-gadolinium-silver alloy. *Corros. Sci.* **2022**, *194*, 109924. [CrossRef]
27. Wu, H.; Shi, Z.; Zhang, X.; Qasim, A.; Xiao, S.; Zhang, F.; Wu, Z.; Wu, G.; Ding, K.; Chu, P. Achieving an acid resistant surface on magnesium alloy via bio-inspired design. *Appl. Surf. Sci.* **2019**, *478*, 150–161. [CrossRef]
28. Zhang, Z.; Zeng, R.; Lin, C.; Wang, L.; Chen, X.; Chen, D. Corrosion resistance of self-cleaning silane/polypropylene composite coatings on magnesium alloy AZ31. *J. Mater. Sci. Technol.* **2020**, *41*, 43–55. [CrossRef]
29. Wu, G.; Zhao, Y.; Zhang, X.; Ibrahim, J.; Chu, P. Self-protection against corrosion of aged magnesium alloy in simulated physiological environment. *Corros. Sci.* **2013**, *68*, 279–285. [CrossRef]

30. Wu, H.; Xiao, S.; Chen, D.; Qasim, A.; Ding, K.; Wu, G.; Chu, P. Effects of diamond-like carbon film on the corrosion behavior of NdFeB permanent magnet. *Surf. Coat. Technol.* **2017**, *312*, 66–74. [CrossRef]
31. Hua, L.; Sun, J.; Wu, G. Enhancing corrosion resistance of hydrothermally-treated magnesium-aluminum alloys by preprocessed metallurgical microstructure. *Thin Solid Film.* **2022**, *752*, 139247. [CrossRef]
32. Zhang, X.; Yuan, G.; Mao, L.; Niu, J.; Ding, W. Biocorrosion properties of as-extruded Mg-Nd-Zn-Zr alloy compared with commercial AZ31 and WE43 alloys. *Mater. Lett.* **2012**, *66*, 209–211. [CrossRef]
33. Mao, L.; Shen, L.; Niu, J.; Zhang, J.; Ding, W.; Wu, Y.; Fan, R.; Yuan, G. Nanophasic biodegradation enhances the durability and biocompatibility of magnesium alloys for the next-generation vascular stents. *Nanoscale* **2013**, *5*, 9517–9522. [CrossRef] [PubMed]
34. Zhang, X.; Yuan, G.; Mao, L.; Niu, J.; Fu, P.; Ding, W. Effects of extrusion and heat treatment on the mechanical properties and biocorrosion behaviors of a Mg-Nd-Zn-Zr alloy. *J. Mech. Behav. Biomed.* **2012**, *7*, 77–86. [CrossRef]
35. Zong, Y.; Yuan, G.; Zhang, X.; Mao, L.; Niu, J.; Ding, W. Comparison of biodegradable behaviors of AZ31 and Mg–Nd–Zn–Zr alloys in Hank's physiological solution. *Mater. Sci. Eng. B* **2012**, *177*, 395–401. [CrossRef]
36. Qin, H.; Zhao, Y.; An, Z.; Cheng, M.; Wang, Q.; Cheng, T.; Wang, Q.; Wang, J.; Jiang, Y.; Zhang, X.; et al. Enhanced antibacterial properties, biocompatibility, and corrosion resistance of degradable Mg-Nd-Zn-Zr alloy. *Biomaterials* **2015**, *53*, 211–220. [CrossRef]
37. Zai, W.; Su, Y.; Man, H.; Lian, J.; Li, G. Effect of pH value and preparation temperature on the formation of magnesium phosphate conversion coatings on AZ31 magnesium alloy. *Appl. Surf. Sci.* **2019**, *492*, 314–327. [CrossRef]
38. Zhang, C.; Liao, S.; Yu, B.; Lu, X.; Chen, X.; Zhang, T.; Wang, F. Ratio of total acidity to pH value of coating bath: A new strategy towards phosphate conversion coatings with optimized corrosion resistance for magnesium alloys. *Corros. Sci.* **2019**, *150*, 279–295.
39. Lv, Y.; Sun, S.; Zhang, X.; Lu, X.; Dong, Z. Construction of multi-layered Zn-modified TiO_2 coating by ultrasound-auxiliary micro-arc oxidation: Microstructure and biological property. *Mater. Sci. Eng. C* **2021**, *131*, 112487. [CrossRef]
40. Liu, X.; He, H.; Zhang, T.; Ouyang, L.; Zhang, Y.; Yuan, S. Superhydrophobic and self-healing dual-function coatings based on mercaptabenzimidazole inhibitor-loaded magnesium silicate nanotubes for corrosion protection of AZ31B magnesium alloys. *Chem. Eng. J.* **2021**, *404*, 127106. [CrossRef]
41. She, Z.; Li, Q.; Wang, Z.; Li, L.; Chen, F.; Zhou, J. Novel method for controllable fabrication of a superhydrophobic CuO surface on AZ91D magnesium alloy. *ACS Appl. Mater. Interfaces* **2012**, *4*, 4348–4356. [CrossRef] [PubMed]
42. Lu, Z.; Wang, P.; Zhang, D. Super-hydrophobic film fabricated on aluminium surface as a barrier to atmospheric corrosion in a marine environment. *Corros. Sci.* **2015**, *91*, 287–296. [CrossRef]